INTERNATIONAL JOURNAL OF HYDROGEN ENERGY 40 (2015) 16383–16390

Available online at www.sciencedirect.com

ScienceDirect

journal homepage: www.elsevier.com/locate/he

NaMgH$_3$ a perovskite-type hydride as advanced hydrogen storage systems: Electronic structure features

A.H. Reshak [a,b,*]

[a] New Technologies - Research Centre, University of West Bohemia, Univerzitni 8, 306 14 Pilsen, Czech Republic
[b] Center of Excellence Geopolymer and Green Technology, School of Material Engineering, University Malaysia Perlis, 01007 Kangar, Perlis, Malaysia

ARTICLE INFO

Article history:
Received 31 August 2015
Received in revised form
7 October 2015
Accepted 8 October 2015
Available online 24 October 2015

Keywords:
Hydrogen storage
NaMgH$_3$
DFT
Electronic charge density

ABSTRACT

The physical properties of perovskite NaMgH$_3$ has been comprehensively investigated by means of density functional theory. Calculations reveals that NaMgH$_3$ is a wide band gap insulator. The angular momentum projected density of states and the valence electronic charge density explore that the NaMgH$_3$ has high gravimetric and volumetric H densities. The calculated angular momentum projected density of states reveals that the hydrogen posses the highest density among Mg and Na. It has been found that a charge transfer occurs towards H atom. Complex first-order linear optical properties helps to further understand the physical properties of NaMgH$_3$. Analyzing the optical properties reveals the NaMgH$_3$ posses negative uniaxial anisotropy and the optical properties give deep insight into the electronic structure.

Introduction

In the recent years there is a tremendous increase in energy consumption, and more than 80% of all the energy is taken from the fossil fuels; like crude oil, coal and natural gas. These fossil fuels are not renewable and one day will be vanishes. Moreover they cause increase in the CO_2 concentration in the atmosphere. This is probably the main reason of rising temperatures, global worming, changing the climate. The top ten of the most important problems that the humanity should solve in the nearest future is the clean energy to improve the air quality in congested cities and as acceptable good alternative power sources for the future. Several based complex hydrides materials were comprehensively investigated to explore their suitability and stability as hydrogen strong materials at moderate pressures and temperatures [1–7]. For instance Brik and Kityk [8] investigated the structural, electronic, optical and elastic properties of lithium amide $LiNH_2$ crystal as promising hydrogen storage materials. Therefore, search for novel hydrogen storage materials is still desirable. Among the good materials which are suitable and stabile as hydrogen strong materials are the perovskite-type hydride. These material have the chemical formula ABX_3, where A and B are cations while X is the anion. Ikeda et al. [9–12] have extensively investigated the reversible hydriding and dehydriding reactions, thermodynamical stability of perovskite-type

* New Technologies - Research Centre, University of West Bohemia, Univerzitni 8, 306 14 Pilsen, Czech Republic.
E-mail address: maalidph@yahoo.co.uk.
http://dx.doi.org/10.1016/j.ijhydene.2015.10.030
0360-3199/

hydride $NaMgH_3$ and $Li_xNa_{1-x}MgH_3$ (x = 0.0, 0.5 and 1.0). It has been found that $NaMgH_3$ has high gravimetric and volumetric H densities ($\rho_G \approx 6\%$ and $\rho_v \approx 88$ kg/m^3) and reversible hydriding and dehydriding reactions therefore, it considered as a promising candidate for hydrogen storage applications. Xiao et al. [13] have investigated the thermodynamic and electronic properties of $Li_xNa_{1-x}MgH_3$ (x = 0.0, 0.25, 0.5 and 7.5) using the density functional theory (DFT) based on VASP code within the generalized-gradient approximation (GGA). The obtained results suggested that Li substitution in $NaMgH_3$ results in a favorable modification for onboard hydrogen storage applications. Komiya et al. [14] have synthesize perovskite-type hydrides $MMgH_3$ (M = Na, K, Rb) by using ball-milling. They reported that these materials are decomposed at temperatures between 673 and 723 K in several ways depending on M. Two provskite related metal hydrides $NaMgH_3$ and Na_3AlH_3 were structurally investigated by Ronnebro et al. [15] using powder diffraction techniques. Bouamrane et al. [16] have used direct reaction of hydrogen on mixture of Na + Mg or NaF + Mg for synthesis the $NaMgH_3$ and $NaMgH_2F$. First principles calculations based on VASP code within the generalized gradient approximation were performed to investigate the structural stability of $MMgH_3$ (M = Li,Na, K, Rb, Cs) compounds [17]. Pottmaier et al. [18] have presented comprehensive characterization of $NaMgH_3$ with respect to structural and thermodynamic properties.

The above investigations reveals that $NaMgH_3$ is one of the suitable and stabile hydrogen storage materials at moderate pressures and temperatures [9–18]. Moreover the previous DFT calculations on $NaMgH_3$ were performed using non-full potential method within GGA. This motivated us to perform a first principle calculation for $NaMgH_3$ using DFT based on all-electron full-potential method within the recently modified Becke-Johnson potential (*mBJ*) [19] to investigate the electronic band structure, total and partial density of states, valence electronic charge distribution and the chemical bonding characters. Furthermore, deep insight into the electronic band structure can be obtained from the optical transitions therefore, we have calculated the complex first-order linear optical properties of $NaMgH_3$. In such calculation the energy eigenvalues and electron wave functions were involved. Thus, the obtained optical properties are natural outputs of band structure calculations. Therefore, as a natural extension to existence information a detailed depiction of the optical properties is timely and would bring us important insights in understanding the origin of the band structure. It is well known that DFT within GGA cause to underestimated the band gap, since the investigation of the structural properties of such materials need accurate results therefore, it is necessary to use an accurate exchange correlation potential such like GW approximation [20] or the recently modified Becke-Johnson potential (*mBJ*) to obtain an accurate band splitting and hence accurate band gap value. Due to the improvement in the computational technologies, the first-principles calculation has proven to be one of the powerful and useful tools to predict the crystal structure and its properties which are related to the electron configuration of a material before its synthesis [21–24].

Details of calculation

Several research groups have synthesized and characterized $NaMgH_3$, the reported x-ray diffraction data show that $NaMgH_3$ crystallizes in orthorhombic space group *Pnma* with the lattice parameters a = 5.4634 Å, b = 7.7030 Å and c = 5.4108 Å [16]. The experimental crystal structure [16] was optimized using the full potential linear augmented plane wave plus local orbitals (*FPLAPW* + *lo*) method as implemented in WIEN2k package [25]. Since the generalized gradient approximation (*PBE* − *GGA*) [26] exhibits better equilibrium structural parameters and energetic of different phases therefore, we have used *PBE* − *GGA* for optimized crystal structure. The atomic positions were optimized by minimizing the forces acting on the atoms. The optimized crystal structure are listed in Table 1 in comparison with the experimental data [16] and previous theoretical results [13,17]. The crystal structure of $NaMgH_3$ is illustrated in Fig. 1 which shows the [MgH_6] octahedra arrangement with the Na ions. We have used the relaxed geometry to calculate the electronic structure, the chemical bonding, electronic charge density and the optical properties using *PBE* − *GGA* and *mBJ*. The total and partial density of states (DOS) were calculated by means of the modified tetrahedron method [27]. The input required for calculating the DOS are the energy eigenvalues and eigenfunctions which are the natural outputs a band structure calculation. The total DOS and partial DOS are calculated for a large energy range (−9.0 eV up to 15.0 eV). The states below the Fermi energy (E_F) are the valence states and states above E_F are the conduction states. Hence we obtain DOS for both valence and conduction band states. The potential for the construction of basis functions inside the sphere of the muffin tin was spherically symmetric, whereas outside the sphere it was constant [28]. The radius of the muffin tin spheres (R_{MT}) have been chosen to be 2.14 a.u. for Mg, 2.5 a.u. for Na and 1.15 a.u. for H. The basis functions inside the interstitial region were expanded up to $R_{MT} \times K_{max} = 7.0$ and inside the atomic spheres for the wave function, in order to achieve the total energy convergence. The potential for the construction of basis functions inside the sphere of the muffin tin was spherically symmetric, whereas outside the sphere it was constant [28]. The maximum value of l were taken as $l_{max} = 10$, while the charge density is Fourier expanded up to $G_{max} = 12.0(a.u)^{-1}$. Self-consistency is obtained using 200 $\vec{k}$ points in the irreducible Brillouin zone (*IBZ*). The self-consistent calculations are converged since the total energy of the system is stable within 0.00001 Ry. The electronic band structure and the related properties were performed within 1000 $\vec{k}$ points in the *IBZ*.

Results and discussion

Electronic band structure, density of states and valence electronic charge density

The calculated total and Na-2s/2p, Mg-3s/2p and H-s partial density of states along with the calculated electronic band structure were illustrated in Fig. 2. It is clear that the valence

Table 1 – Optimized crystal structure in comparison with the experimental data [16] and the previous theoretical calculations [13,17].

Cell parameters (Å)	a		b		c	
Exp.	5.4634[a]		7.7030[a]		5.4108[a]	
This work	5.4568		7.6968		5.3779	
Previous work	5.4094[b]		7.6262[b]		5.3328[b]	
	5.4525[c]		7.6952[c]		5.3683[c]	
Atomic positions						
atom	x exp.	x optim.	y exp.	y optim.	z exp.	z optim.
Na (4c)	0.030	0.023	0.25	0.25	0.006	0.006
Mg (4b)	0.0	0.0	0.0	0.0	0.5	0.5
H1 (4c)	0.524	0.505	0.25	0.25	0.081	0.082
H2 (8d)	0.292	0.298	0.042	0.036	0.793	0.769

[a] Ref. [16].
[b] Ref. [13].
[c] Ref. [17].

band maximum (VBM) is mainly originated from H-s, with small contributions from Na-2p, Mg-3s/2p states, while the conduction band minimum (CBM) from Na-2s with small contributions from Na-2p, Mg-3s/2p states. The calculated energy band gap is about 3.22 eV (*PBE – GGA*) and 3.60 eV (*mBJ*). The later exhibit an energy band gap better than the previous calculations (3.45 eV [17] 3.52 eV [13]) using VASP code within *PBE – GGA*. It is well known that *PBE – GGA* underestimated the energy band gap. In order to get accurate band gap's value one should go beyond the usual *PBE – GGA*. Therefore, we have used the recently modified Becke-Johnson potential [19]. To the best of our knowledge, no experimental gap's value for $NaMgH_3$ is available in the literature to make a meaningful comparison with our theoretical results. Therefore, based on

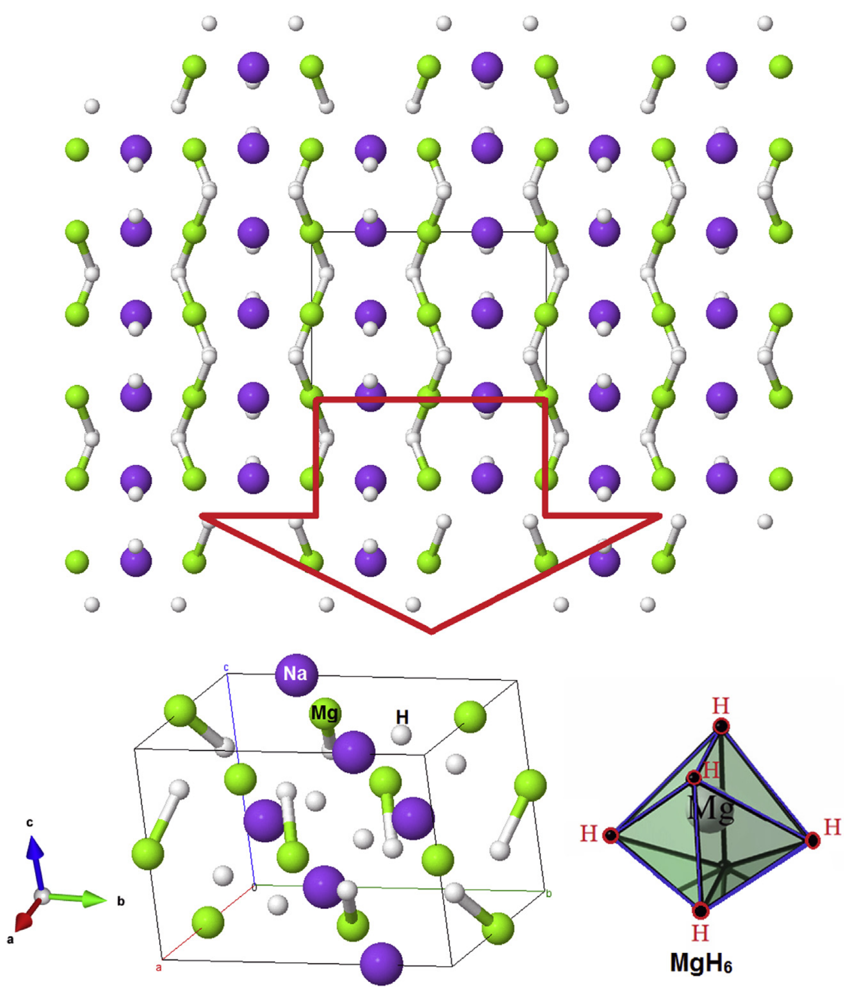

Fig. 1 – The crystal structure of $NaMgH_3$ and the unit cell. It shows the $[MgH_6]$ octahedra arrangement with the Na ions.

our previous experiences with using *mBJ* [19], we expected the obtained *mBJ*-gap is closer to the expected measured one. Future experimental work will testify our calculated results. It has been noticed that from the calculated angular momentum projected density of states the density of states below Fermi level (E_F) are mixture of Na-2s/2p, Mg-3s/2p, H1-s and H2-s states, where H1-s and H2-s are strongly hybridized along the whole energy region below E_F, whereas Na-2p, Mg-3s/2p states are hybridized at the VBM only. The energy region from the CBM and above are formed by mixture of Na-2s/2p, Mg-3s/2p, H1-s and H2-s states with almost no hybridization between the states except in the energy region between 4.0 and 4.5 eV where H1-s and H2-s hybridized and exhibit insignificant contribution to the empty states.

The angular momentum decomposition of the atoms projected electronic density of states below the Fermi level of $NaMgH_3$ helps to elucidate the characters of chemical bonding. Therefore, the total number of electrons per electron Volts (e/eV) for Na-2s/2p, Mg-3s/2p, H1-s and H2-s orbitals can be obtained from Fig. 2. The total number of e/eV for H1-1s orbital is 0.5 e/eV, H1-1s orbital is 0.35 e/eV, Na-2s orbital is 0.05 e/eV, Mg-2p orbital is 0.12 e/eV, Mg-3s orbital is 0.08 e/eV and Na-2p orbital is 0.038 e/eV. Thus there are some electrons from Na, Mg and H atoms are transferred into the valence bands to form covalence interactions between Na, Mg and H atoms. This interaction depends on the degree of the hybridization and the electronegativity differences. The electronegativity of Na, Mg and H are 0.93, 1.31 and 2.2 according to Pauling electronegativity scale. To further understanding the chemical bonding characters, the total valence bands electronic charge density distribution were calculated in two different crystallographic planes as illustrated in Fig. 3(a)–(c). It has been found that the interaction between Na and MgH_6 units is pure ionic while Mg and H interaction exhibit ionic-covalent characters as it is clear from (1 0 0) and (1 0 1) crystallographic planes. Both counter plots exhibit that the H atoms are surrounding by uniform spherical charge, to illustrate this we have taken an clear image for the area around H atom (see Fig. 3(c)). This figure confirm that there is a charge transfer towards H atoms as shown by the maximum charge surrounding H atoms (blue color refer to the maximum charge accumulation). In addition we have calculated the bond lengths as listed in Table 2 in comparison with the experimental data [16], good agreement was found.

Complex first-order linear optical dispersion

To further understanding the physical properties of $NaMgH_3$ the optical properties are also investigated. Calculations of the optical dielectric functions involve the energy eigenvalues and electron wave-functions which are natural outputs of band structure calculations. The allowed optical transitions according to the dipolar selection rule, which state that only transitions changing the angular momentum quantum number l by unity ($\Delta = \pm 1$) are allowed, can give a clear map for the electronic band structure of the materials. Therefore, we have calculated the complex first-order linear optical properties to get further information about the band dispersions so as to support our previous observations. The expressions for calculating the imaginary part of the complex first-order linear optical dielectric functions are give elsewhere [29]. The imaginary and real parts of the optical dielectric functions along the polarization directions [100], [010] and [001] are illustrated in Fig. 4(a).

The energy band gap can be obtained directly from the imaginary part dispersions through the absorption edges of the optical components $\varepsilon_2^{xx}(\omega)$, $\varepsilon_2^{yy}(\omega)$ and $\varepsilon_2^{zz}(\omega)$. It has been found that the optical gap is about 3.60 eV. While it can be obtained indirectly from the real parts $\varepsilon_1^{xx}(\omega)$, $\varepsilon_1^{yy}(\omega)$ and $\varepsilon_1^{zz}(\omega)$ from the calculated values of $\varepsilon_1^{xx}(0)$, $\varepsilon_1^{yy}(0)$ and $\varepsilon_1^{zz}(0)$ based on Penn model $\varepsilon(0) \approx 1 + (\hbar\omega_P/E_g)^2$ [30]. Penn proposed a relation between $\varepsilon(0)$ and E_g, E_g is some kind of averaged energy gap which could be related to the real energy gap. Thus the imaginary and real parts helps to find the energy band gap value. There are some other important features can be obtained from the real part for instance the plasmon oscillations ω_p^{xx}, ω_p^{yy} and ω_p^{zz}. These are associated with inter-band transitions. The plasmon maximum is usually the most intense

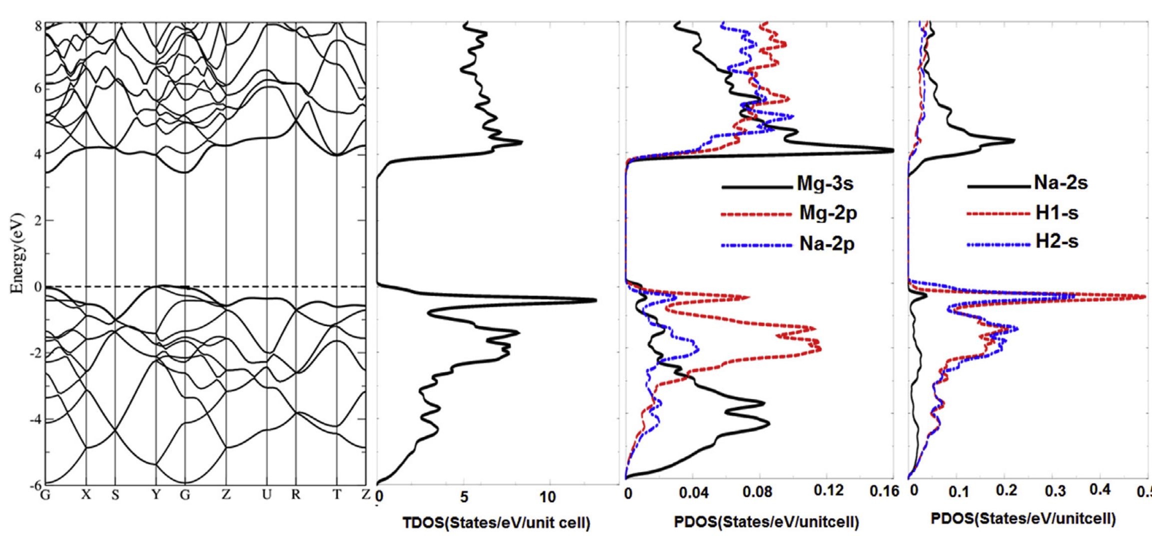

Fig. 2 – (a) Calculated band structure along with the total and Na2s/2p, Mg-3s/2p and H-1s partial density of states of $NaMgH_3$.

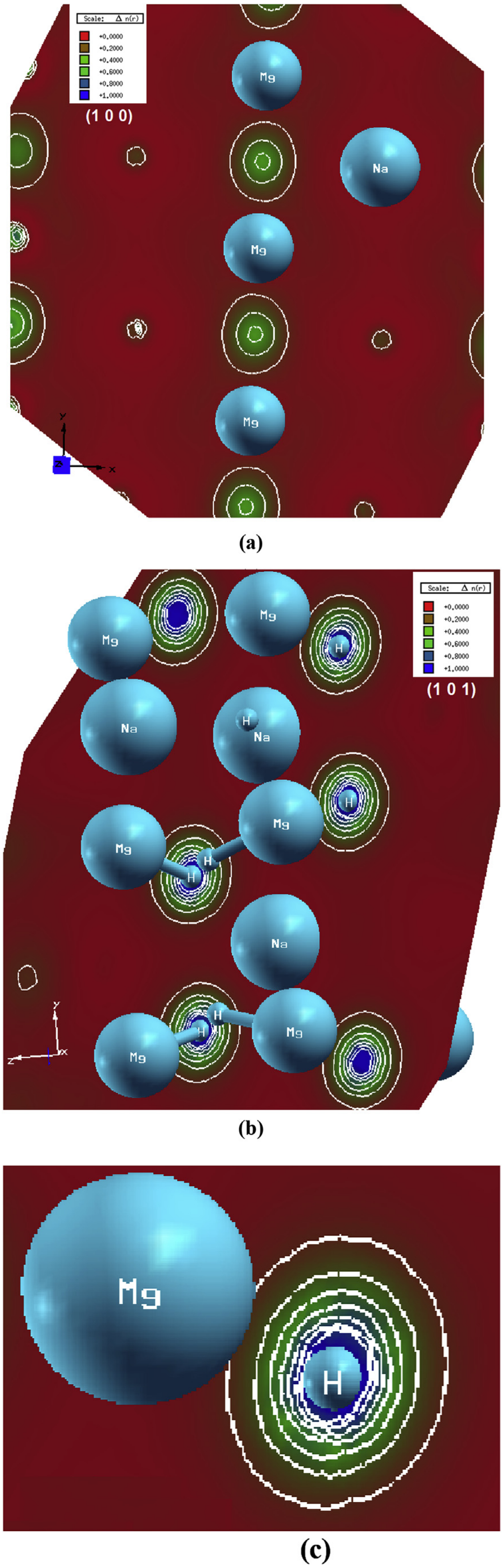

Fig. 3 – Calculated valence electronic charge density distribution in different crystallographic planes, it shows the [MgH_6] octahedra arrangement with the Na ions; (a) crystallographic plane (1 0 0); (b) crystallographic plane (1 0 1); (c) show the charge transfer towards H atom indicated by the blue color surrounding H atoms, according to thermoscale the blue color indicate the maximum charge accumulation. (For interpretation of the references to colour in this figure legend, the reader is referred to the web version of this article.)

Table 2 – Some selected bond lengths in comparison with the experimental data [16] and previous work [17].

Bonds	Bond lengths (this work)	Bond lengths (exp.)	Bond lengths (previous work)
Mg–H1	1.97	1.99 (1)	1.977
Mg–H2	2.23	2.24 (5)	1.967
Mg–H3	1.73	1.75 (5)	1.968
Na–H1	2.85	2.87 (4)	2.302
Na–H2	2.47	2.49 (5)	2.326

Exp. Ref. [16].
Previous work Ref. [17].

feature in the spectrum and this is at energy where $\varepsilon_1^{xx}(\omega)$, $\varepsilon_1^{yy}(\omega)$ and $\varepsilon_1^{zz}(\omega)$ crosses zero which is associated with the existence of plasma oscillations. The values of $\varepsilon_1^{xx}(0)$, $\varepsilon_1^{yy}(0)$, $\varepsilon_1^{zz}(0)$, ω_p^{xx}, ω_p^{yy} and ω_p^{zz} are listed in Table 3. Further, the uniaxial anisotropy ($\delta\varepsilon$) can be obtained from $\varepsilon_1^{xx}(0)$, $\varepsilon_1^{yy}(0)$ and $\varepsilon_1^{zz}(0)$. It has been found that $NaMgH_3$ posses negative $\delta\varepsilon$ which reveals that $NaMgH_3$ exhibit weak anisotropic nature. Deep insight into the electronic structure can be obtained from further analyzing to the imaginary part of the optical dielectric function. The first critical points (absorption edges) are belong to the optical transitions between the valence states H-1s, Mg-3s/2p, Na-2p and the conduction states Na-2s, Mg-3s/2p, Na-2p. While the fundamental peak is belong to the optical transitions H-1s, Mg-3s/2p, Na-2s/2p of the valence band and H-1s, Mg-3s/2p, Na-2s/2p of the conduction bands. Thus the optical transitions can give clear picture about the energy band dispersion. Therefore, we can use our calculated electronic band structure and the partial density of states to identify these transitions (see Fig. 4(b)). We have divided the optical transitions into three energy regions as A (0.0–5.0) eV, B (5.0–10.0) eV and C (10.0–14.0) eV (see Fig. 4(b)). According to the band to band transitions we can identify the origin of the orbitals which are responsible on each optical transition and hence the spectral structures of $\varepsilon_2^{xx}(\omega)$, $\varepsilon_2^{yy}(\omega)$ and $\varepsilon_2^{zz}(\omega)$.

From the calculated imaginary $\sigma^2(\omega)$ and real $\sigma_1(\omega)$ parts of the optical conductivity as shown in Fig. 4(c) we can gain further information about the origin of the electronic structure since the optical conductivity is directly related to the complex dielectric function $\varepsilon(\omega) = \varepsilon_1(\omega) + i\varepsilon_2(\omega)$. In the energy region confined between 0.0 and ω^p, the imaginary part of the

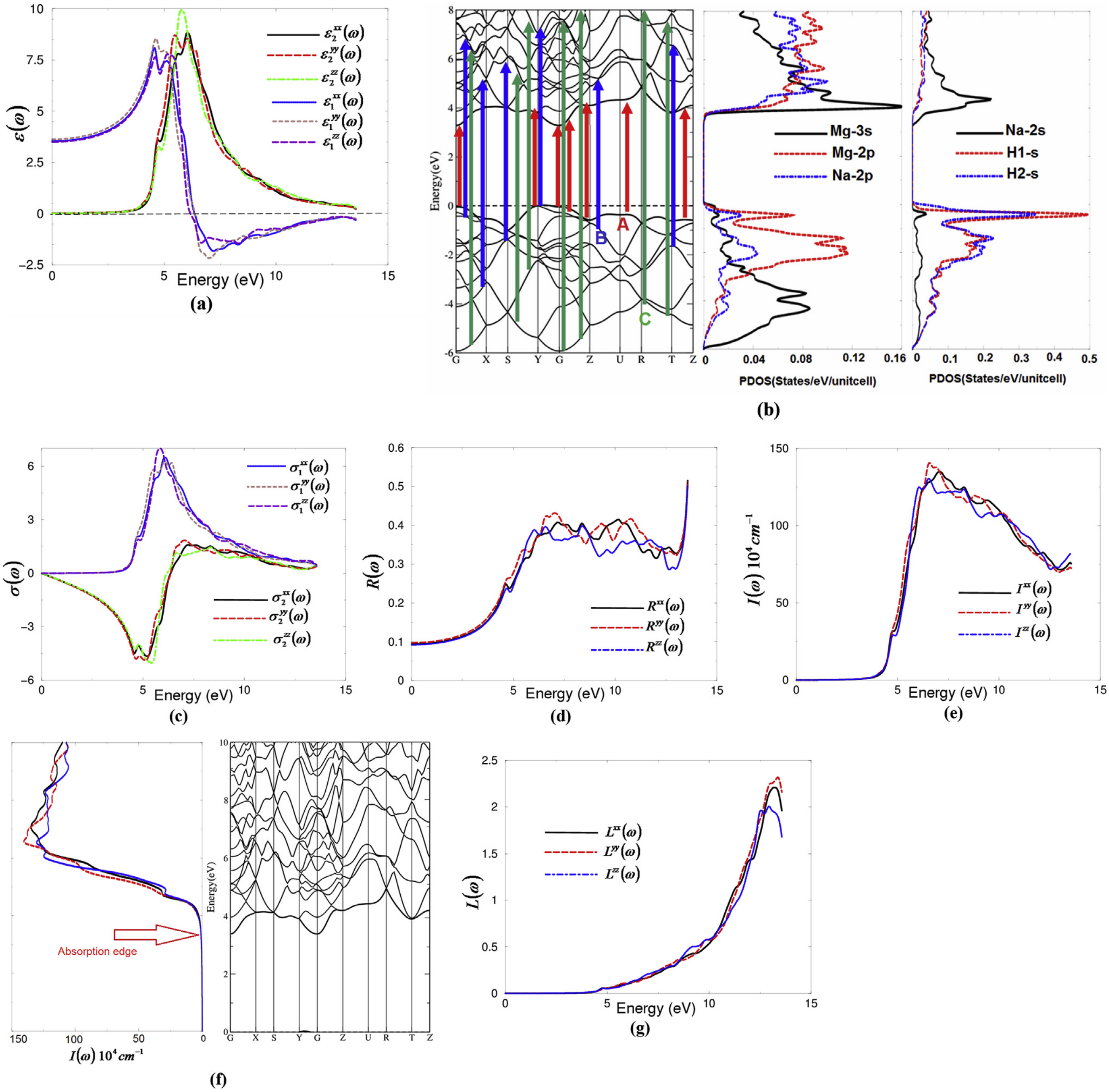

Fig. 4 – (a) Calculated $\varepsilon_2^{xx}(\omega)$ (dark solid curve-black color online), $\varepsilon_2^{yy}(\omega)$ (light long dashed curve-red color online) and $\varepsilon_2^{zz}(\omega)$ (light dotted dashed curve -green color online) along with Calculated $\varepsilon_1^{xx}(\omega)$ (dark solid curve-blue color online), $\varepsilon_1^{yy}(\omega)$ (light dashed curve-brown color online) and $\varepsilon_1^{zz}(\omega)$ (light sold curve -violet color online); (b) The optical transitions depicted on a generic band structure along with the Na2s/2p, Mg-3s/2p and H-1s partial density of states for $NaMgH_3$. For simplicity, we have labeled the optical transitions as A, B, and C. The transitions (A) are responsible for the structures for $\varepsilon_2^{xx}(\omega)$, $\varepsilon_2^{yy}(\omega)$ and $\varepsilon_2^{zz}(\omega)$ in the spectral range 0.0–5.0 eV; the transitions (B) 5.0–10.0 eV, and the transitions (C) 10.0–14.0 eV; (c) Calculated $\sigma_2^{xx}(\omega)$ (dark solid curve-black color online), $\sigma_2^{yy}(\omega)$ (light dashed curve-red color online) and $\sigma_2^{zz}(\omega)$ (light dotted dashed curve -green color online) along with Calculated $\sigma_1^{xx}(\omega)$ (dark solid curve-blue color online), $\sigma_1^{yy}(\omega)$ (light dashed curve-red brown online) and $\sigma_1^{zz}(\omega)$ (light solid curve - violet color online) for $NaMgH_3$; (d) Calculated $R^{xx}(\omega)$ (dark solid curve-black color online), $R^{yy}(\omega)$ (light dashed curve-red color online), and $R^{zz}(\omega)$ (light dotted dashed curve -blue color online) for $NaMgH_3$; (e) Calculated absorption coefficient $I^{xx}(\omega)$ (dark solid curve-back color online), $I^{yy}(\omega)$ (light dashed curve-red color online) and $I^{zz}(\omega)$ (light dotted dashed curve -blue color online) spectrum for $NaMgH_3$ the absorption coefficient in 10^4 cm^{-1}; (f) calculated electronic band structure along with the calculated absorption coefficient. It has been noticed that the absorption edges matched the energy band gap of the electronic band structure; (g) Calculated loss function $L^{xx}(\omega)$ (dark solid curve-back color online), $L^{yy}(\omega)$ (light dashed curve-red color online) and $L^{zz}(\omega)$ (light dotted dashed curve -blue color online) spectrum for $NaMgH_3$. (For interpretation of the references to colour in this figure legend, the reader is referred to the web version of this article.)

Table 3 – The calculated energy band gap in comparison with the previous calculation [16,12], $\varepsilon_1^{xx}(0)$, $\varepsilon_1^{yy}(0)$, $\varepsilon_1^{zz}(0)$, $\varepsilon_1^{average}(0)$, $\delta\varepsilon$, ω_p^{xx}, ω_p^{yy}, ω_p^{zz}. These parameters are calculated within mBJ.

$NaMgH_3$	
Eg (eV)	3.22 (PBE-GGA)[a], 3.60 (mBJ)[a], 3.45[b], 3.52[c]
$\varepsilon_1^{xx}(0)$	3.547
$\varepsilon_1^{yy}(0)$	3.638
$\varepsilon_1^{zz}(0)$	3.508
$\varepsilon_1^{average}(0)$	3.564
$\delta\varepsilon$	−0.031
ω_p^{xx}	6.381
ω_p^{yy}	6.381
ω_p^{zz}	6.190

[a] This work.
[b] Ref. [17] 3.45 eV.
[c] Ref. [13] 3.52 eV using VASP-GGA.

optical conductivity as represented by $\sigma_2^{xx}(\omega)$, $\sigma_2^{yy}(\omega)$ and $\sigma_2^{zz}(\omega)$ show overturned features of $\varepsilon_2^{xx}(\omega)$, $\varepsilon_2^{yy}(\omega)$ and $\varepsilon_2^{zz}(\omega)$. The real part of the optical conductivity $\sigma_1^{xx}(\omega)$, $\sigma_1^{yy}(\omega)$ and $\sigma_1^{zz}(\omega)$ in general show similar features to that of $\varepsilon_2^{xx}(\omega)$, $\varepsilon_2^{yy}(\omega)$ and $\varepsilon_2^{zz}(\omega)$. The calculated optical reflectivity (Fig. 4(d)) exhibit that $NaMgH_3$ posses low optical reflectivity of about 10.0% at low energy region. The reflectivity increases to 45.0% at around 6.38 eV (plasma resonance) confirming the occurrence of a collective plasmon resonance. At high energies (13.5 eV) the optical reflectivity reach it maximum of about 50.0%. The optical absorption (Fig. 4(e)) show that in the energy region between 0.0 and 3.60 eV the $NaMgH_3$ posses an opaque area. Above 3.60 eV the absorption edge allowed to reach the maximum absorption at the values of the plasma resonance (ω_p^{xx}, ω_p^{yy} and ω_p^{zz}). Fig. 4(e) reveals the origin of the absorption edges associated to the electronic band structure. It is clear that $NaMgH_3$ compound posses wide optical transparency region. Fig. 4(g) show that $NaMgH_3$ posses a strong lossless region around 12.5 eV in concordance with Fig. 4(a,c-f). This lossless region confirms the occurrence of a collective plasmon resonance.

Conclusions

Using the full potential method within the recently modified Becke-Johnson potential, we have investigated the physical properties of the rich hydrogen $NaMgH_3$ to explore its suitability and stability as hydrogen storage material. The calculations reveals that $NaMgH_3$ is a wide band gap insulter. The calculated angular momentum projected density of states explore that the hydrogen posses the highest density among Mg and Na. It has been found that the interaction between Na and MgH_6 units is pure ionic while Mg and H interaction exhibit ionic-covalent characters as it is clear from (100) and (101) crystallographic planes. Both counter plots exhibit that the H atoms are surrounding by uniform spherical charge, which confirm that there is a charge transfer towards H atoms as shown by the maximum charge surrounding H atoms. The calculated bond distance agree well with the measured one. The optical properties helps to gain deep insight into the electronic structures so as further understanding to the atomic arrangement can be obtained. The absorption coefficient confirm the energy gap value and the negative uniaxial anisotropy reveals that $NaMgH_3$ exhibit isotropic nature at low and high energies.

Acknowledgments

The result was developed within the CENTEM project, reg. no. CZ.1.05/2.1.00/03.0088, cofunded by the ERDF as part of the Ministry of Education, Youth and Sports OP RDI programme and, in the follow-up sustainability stage, supported through CENTEM PLUS (LO1402) by financial means from the Ministry of Education, Youth and Sports under the "National Sustainability Programme I. Computational resources were provided by MetaCentrum (LM2010005) and CERIT-SC (CZ.1.05/3.2.00/08.0144) infrastructures.

REFERENCES

[1] Block J, Gray AP. The thermal decomposition of lithium aluminum hydride. Inorg Chem 1965;304:4.
[2] Dilts JA, Ashby EC. Thermal decomposition of complex metal hydrides. Inorg Chem 1972;11:1230.
[3] Bogdanovic B, Schwickardi M. Ti-doped alkali metal aluminium hydrides as potential novel reversible hydrogen storage materials. J Alloys Compd 1997;1:253–5.
[4] Bogdanovic B, Brand RA, Marjanovic A, Schwikardi M, Tolle J. Metal-doped sodium aluminium hydrides as potential new hydrogen storage materials. J Alloys Compd 2000;302:36.
[5] Brinks HW, Hauback BC, Norby P, Fjellvag H. The decomposition of LiAlD4 studied by in-situ X-ray and neutron diffraction,. J Alloys Compd 2003;351:222.
[6] Jensen CM, Gross K. Development of catalytically enhanced sodium aluminum hydride as a hydrogen storage material. J Appl Phys A 2001;72:213.
[7] Morioka H, Kakizaki K, Chung SC, Yamada A. Reversible hydrogen decomposition of KAlH4. J Alloys Compd 2003;353:310.
[8] Brik MG, Kityk IV. Ab initio analysis of the optical, electronic and elastic properties of the hydrogen-storage single crystals LiNH2. Mater Chem Phys 2011;130:685–9.
[9] Ikeda K, Kogure Y, Nakamori Y, Orimo S. Formation region and hydrogen storage abilities of perovskite-type hydrides. Prog Solid State Chem 2007;35:329–37.
[10] Ikeda K, Kato S, Shinzato Y, Okuda N, Nakamori Y, Kitano A, et al. Thermodynamical stability and electronic structure of a perovskite-type hydride, NaMgH3. Journal of Alloys Compd 2007;446–447:162–5.
[11] Ikeda K, Kogure Y, Nakamori Y, Orimo S. Reversible hydriding and dehydriding reactions of perovskite-type hydride NaMgH3. Scr Mater 2005;53:319–22.
[12] Ikeda K, Nakamori Y, Orimo S. Formation ability of the perovskite-type structure in LixNa1 − xMgH3 (x = 0, 0.5 and 1.0). Acta Mater 2005;53:3453–7.
[13] Xiao Xiao-Bing, Tang Bi-Yu, Liao Sun-Qi, Peng Li-Ming, Ding Wen-jiang. Thermodynamic and electronic properties of quaternary hydrides LixNa1−xMgH3. J Alloys Compd 2009;474:522–6.
[14] Komiya K, Morisaku N, Rong R, Takahashi Y, Shinzato Y, Yukawa H, et al. Synthesis and decomposition of perovskite-

type hydrides, MMgH3 (M = Na, K, Rb). J Alloys Compd 2008;453:157–60.
[15] Ronnebro Ewa, Noreus Dag, Kadir Karim, Reiser Alexander, Bogdanovic Borislav. Investigation of the perovskite related structures of NaMgH3, NaMgF3 and Na3AlH6. J Alloys Compd 2000;299:101–6.
[16] Bouamrane A, Laval JP, Soulie J-P, Bastide JP. Structural charactrization of NaMgH2F and NaMgH3. Mater Res Bull 2000;35:545–9.
[17] Vajeeston P, Ravindran P, Kjekshus A, Fjellvag H. First-principles investigations of the MMgH3 (M=Li, Na, K, Rb, Cs) series. J Alloys Compd 2008;450:327–37.
[18] Pottmaier Daphiny, Pinatel Eugenio R, Vitillo Jenny G, Garroni Sebastiano, Orlova Maria, Dolors Baro Maria, et al. Structure and thermodynamic properties of the NaMgH3 perovskite: a comperhensive study. Chem Mater 2011;23:2317–26.
[19] Tran F, Blaha P. Accurate band gaps of semiconductors and insulators with a semilocal exchange-correlation potential. Phys Rev Lett 2009;102 226401.
[20] Gygi F, Baldereschi A. Quasiparticle energies in semiconductors: self-energy correction to the local-density approximation. Phys Rev Lett 1989;62:2160.
[21] Reshak AH. MgH2 and LiH metal hydrides crystals as novel hydrogen storage material: electronic structure and optical properties. Int J Hydrogen Energy 2013;38:11946–54. Plucinski, K. J.; Kityk, I. V.; Kasperczyk, J.; Sahraoui, B., The structure and electronic properties of silicon oxynitride gate dielectrics, Semiconductor Science and Technology 16, 467-470(2001).
[22] Malachowski M, Kityk IR, Sahraoui B. Electronic structure and optical response in $Ga_xAl_{1-x}N$ solid alloys. Phys Lett A 1998;242:337–42.
[23] Fuks-Janczarek I, Miedzinski R, Brik MG, Majchrowski A, Jaroszewicz LR, Kityk IV. Z-scan analysis and ab initio studies of beta-BaTeMo2O9 single crystal. Solid State Sci 2014;27:30–5.
[24] Ma C-G, Brik MG. First principles studies of the structural, electronic and optical properties of LiInSe2 and LiInTe2 chalcopyrite crystals. Solid State Commun 2015;203:69–74.
[25] Blaha P, Schwarz K, Madsen GKH, Kvasnicka D, Luitz J. WIEN2k, an augmented plane wave plus local orbitals program for calculating crystal properties. Austria: Vienna University of Technology; 2001.
[26] Perdew JP, Burke S, Ernzerhof M. Generalized gradient approximation made simple. Phys Rev Lett 1996;77:3865.
[27] Blöchl PE, Jepsen O, Andersen OK. Improved tetrahedron method for brillouin-zone integrations. Phys Rev B Condens Matter 1994;49(23):16223–33.
[28] Schwarz K, Blaha P. Solid state calculations using WIEN2k. Comput Mater. Sci 2003;28:259.
[29] Khan MA, Kashyap Arti, Solanki AK, Nautiyal T, Auluck S. Interband optical properties of Ni3Al. Phys Rev B 1993;23:16974.
[30] Penn DR. Wave-number-dependent dielectric function of semiconductors. Phys Rev B 1962;128:2093.